A kinetic-based zeolite PRB design method for remediating groundwater polluted by high NH_4^+ MSW leachate considering spatio-temporal concentration evolutions

Yi-Xin Yang [a], Jia-Kai Chen [a], Li Zhao [a], Yu-Qing You [a], Ze-Jian Chen [b],
Jun-Nan Cao [c], Fei Liu [d], Shuai Zhang [a], Liang-Tong Zhan [a], Yun-Min Chen [a],
Bate Bate [a,*]

[a] Institute of Geotechnical Engineering, Zhejiang University, Hangzhou, China
[b] Department of Civil and Environmental Engineering, The Hong Kong Polytechnic University, Kowloon, Hong Kong
[c] Department of Civil Engineering and Construction, Georgia Southern University, USA
[d] Department of Environmental Sciences and Engineering, China University of Geoscience (Beijing), Beijing, China

ARTICLE INFO

ABSTRACT

Albeit the widely-used zeolite permeable reactive barriers (PRBs) in remediating ammonium in groundwater from mining industry and municipal solid waste landfills, the engineering design is primarily based on the traditional maximum adsorption capacity method and the residence time method. Both methods could predict neither the NH_4^+ saturation versus time evolution, nor the breakthrough behavior of a zeolite PRB. This adds uncertainty to the PRB performance, on top of the conventional clogging and preferential flow problems. In this study, a kinetic-based method was proposed to tackle above challenges. An adsorption kinetic model was obtained based on two-variables batch test results, whereas the rate constant k was 0.1728 L/(min · mol), and the adsorption exponents with respect to both NH_4^+ concentration and the zeolite adsorption site molarity were unity. Effective diffusion coefficient D^* (1×10^{-9} m^2/s) and mechanical dispersion ($\alpha_L = 8 \times 10^{-3}$ m) were calibrated by Cl$^-$ tracer tests. Three column tests with inlet NH_4^+ concentrations of 200, 1000 and 2000 mg/L were performed to obtain the breakthrough curves, which agreed well ($R^2 > 0.93$) with those simulated by the proposed method. Indeed, breakthrough curves considering kinetics were also more precise than those with instantaneous adsorption assumption ($R^2 = 0.712$-0.863). The proposed method was used for calculating the required thickness of a PRB for a municipal solid waste landfill, which was more conservative than those calculated by traditional methods.

1. Introduction

Municipal solid wastes (MSW) landfills are ubiquitous in China, USA, and many other developing countries. There are 27,000 unlined MSW landfills in China (Ye et al., 2019). The leachates from MSW landfills are a major challenge in the United States. Organic matter, ammonium, metals are 3 major contaminant types of MSW landfill leachates (Ye et al.,

2019; Han et al., 2016). The in-situ remediation technology for MSW landfill leachate contaminated soil and groundwater demand removal of multi-component contaminants, which is tackled preferably by permeable reactive barriers (PRBs), especially on hydrogeological conditions of abundant groundwater flow. This is challenging as traditional permeable reactive barrier usually removes single component contaminants, such as chlorinated solvents by zero-valence iron (Shen and Wilson, 2007; Henderson and Demond, 2007) or activated carbon (Erto et al., 2009; Bortone et al., 2013, 2014), ammonium by zeolite (Chen et al., 2022; Zhang et al., 2022), and iron by calcite (Wang et al., 2016), while multi-layer PRBs is desired. Preliminary research shows that organic matters, often characterized by chemical oxygen demand (COD), are often abundant in fresh leachates, which can be oxidized and adsorbed (Ye et al., 2019; Renou et al., 2008; Kjeldsen et al., 2002). Metal concentrations exceed water quality standards at some sites, which are easily stabilized and removed (Hao et al., 2022; Liang-tong et al., 2022; Hao et al., 2021; Son et al., 2018; Wang et al., 2019). Ammonium, on the other hand, is abundant in old leachates, generated due to anaerobic microbial activities (Ye et al., 2019; Renou et al., 2008; Kjeldsen et al., 2002). Ammonium is not easily removed by activated carbon (AC) (Boopathy et al., 2013) or oxidized (more details in Case Study), posing challenges for its containment and remediation in an engineering field. In an engineering pilot site, the contaminated groundwater was treated in-situ by the following treatments, oxidation of organic matters (CODs), adsorption of residuals of CODs and metal cations by activated carbon, adsorption of ammonium by zeolite. The design of the zeolite layer is the major topic of this study, while interactions of ammonium and AC will be briefly presented in Case Study.

Zeolite is one of the most effective and widely used adsorbents for NH_4^+ containment so far (Chen et al., 2022; Saltali et al., 2007; Cruz et al., 2019). Natural zeolite is composed of cage-like structures of aluminosilicates with high cation-exchange capacity and large surface area, which is capable of removing ammonium cations from aqueous solutions effectively (Karadag et al., 2007, 2008; Obiri-Nyarko et al., 2014). Although the adsorption kinetics of zeolite-NH_4^+ interaction was studied extensively (Soetardji et al., 2015; Suprihatin et al., 2020; Ivanova et al., 2010; He et al., 2019; Pan et al., 2019; Zhao et al., 2016), the majority of which assumed pseudo 1st-order kinetics with respect to either $[NH_4^+]$ or the molarity of zeolite adsorption sites. This results in inaccurate estimation of the design thickness of zeolite barriers. An accurate zeolite-NH_4^+ kinetic model was in dire need for cost-saving and performance prediction in a PRB project.

Traditional PRB thickness design methods include maximum adsorption method and residence time method (Obiri-Nyarko et al., 2014; Chen et al., 2012; Gavaskar, 1999). The maximum adsorption method assumes full utilization of the zeolite adsorption capacity for NH_4^+ in accordance with adsorption isotherm. The residence time is the time required for the reaction between contaminated groundwater and reactive material to achieve the treatment goals, and is often calculated by the number of half-lives (time required for concentration reduction of 50%) required to achieve target breakthrough concentration (10% in this study Woinarski et al., 2006) (Obiri-Nyarko et al., 2014). The maximum adsorption method considers only the adsorption capacity of the zeolite at equilibrium, not the hydrodynamic and kinetic adsorption processes. On the other hand, the residence time method assumes first-order chemical reaction and neglects adsorbate saturation, both of which are not always true. Taking the maximal thickness from the above two methods was often used in PRB design. This PRB design approach leaves out true chemical reaction kinetics, hydrodynamics, and spatiotemporal concentration distribution along the thickness of the PRB, which are needed for filling materials replacement or regeneration and performance prediction. Indeed, besides adsorption kinetics, ammonium transportation in porous media is also governed by advection, diffusion and mechanical dispersion (Shackelford and Rowe, 1998), which can be modeled by 1-D mass transport simulation. Recent PRB projects performed both laboratory tests (isotherms, column tests) and numerical modeling (2-D transportation, multi-objective optimization) (Santonastaso et al., 2018; Katarzyna et al., 2019; Maamoun et al., 2020; Cai et al., 2018). Santonastaso et al. designed the thickness of a PRB filled by AC to remediate thallium (TI)-contaminated aquifer combining the laboratory isotherm tests and 2-D contaminant transport simulation in order to consider complicated flow condition and optimize the configuration of PRB to decrease total cost (Santonastaso et al., 2018). Katarzyna et al. proposed a thickness design method for multi-layered PRB based on laboratory tests and numerical modeling considering the optimization of both thickness and the total cost in order to determine the required PRB thickness with the lowest cost (Katarzyna et al., 2019). Maamoun et al. proposed a method combining the laboratory batch and column tests of several materials and multi-objective optimization to design the PRB thickness for Cr (VI) removal in order to select the most feasible reactive material with long residence time and low cost (Maamoun et al., 2020). Cai et al. applied kinetic models obtained from batch tests and modeling to the design of calcite PRB for fluoride remediation in order to compare the design thicknesses in presence of metal ions (Co, Mn, Cd and Ba) (Cai et al., 2018).

Instantaneous adsorption equilibrium was often assumed in a mass transport simulation (details in Materials and Methods), whereas adsorption kinetics was rarely incorporated. The design method based on 1-D mass transport simulation considering instantaneous adsorption equilibrium depends on the retardation factor (R_d) measure by column breakthrough tests. However, one shortcoming is R_d calibration. The R_d is not a constant but a variable related to concentration and velocity which means that the calibration by column breakthrough tests could be time-consuming. This shortcoming can be overcome if kinetic model is incorporated in the mass transport simulation. To date, however, no attempt was identified in the literature.

The goal of this study is to propose a kinetic reaction-based 1-D mass transport modeling method for the design and performance prediction of a zeolite PRB for removal of NH_4^+ from a contaminated MSW landfill site. The objectives are: (1) to obtain a true adsorption kinetic model for zeolite adsorbing NH_4^+, considering both the ammonium concentration

and the molarity of adsorption sites; (2) to quantify the hydrodynamic parameters of a zeolite column matrix via Cl⁻ tracer tests; (3) to establish a kinetic reaction-based 1-D mass transport model, which was verified by NH_4^+ column breakthrough tests; (4) to design an engineering PRB with the newly-proposed method, and to compare with traditional design methods.

2. Materials and methods

Commercial natural clinoptilolite zeolite (Jinyun county, Zhejiang Province, China) with grain size ranging from 1–2 mm was used. The zeolite was washed thoroughly and immersed in deionized water (DI water) for 24 h to remove impurities, and was then oven-dried before using.

Ammonium solutions from 100 to 2000 mg/L (in terms of nitrogen) were prepared by dissolving ammonium chloride (NH_4Cl) powders (AR, Sinopharm Chemical Reagent Co. Ltd., China) in DI water.

Single variable batch tests were conducted in Erlenmeyer flasks containing ammonium solutions ranging from 100 to 2000 mg/L at fixed zeolite contents (1 g/100 mL and 5 g/100 mL). The flasks were agitated in a temperature-controlled orbital shaker with speed of 200 rpm and temperature at 25 °C. Solution samples were collected at various time intervals in the first 1600 min. Ammonium concentrations were determined by Nessler's reagent spectrophotometry method. The amount of adsorbed ammonium (S_e in mg/g) was calculated by Eq. (1) (Alkan et al., 2007; Bhatnagar et al., 2010; Wang et al., 2007; Englert and Rubio, 2005):

$$S_e = \frac{(C_0 - C_e)V}{m} \tag{1}$$

where C_0 and C_e are the initial and equilibrium concentrations of ammonium, in mg/L, respectively; V is the solution volume, in L; m is the weight of zeolite, in g.

Mineralogical composition of original zeolite was analyzed by X-ray diffraction (XRD) measurement (Bruker D8 Advance diffractometer, Bruker, Germany) with Cu-Kα ($\lambda = 0.154056$ nm) radiation and an angle of incidence ranging from 5° to 90°. The phase and compositions were analyzed by MDI Jade 9 software. Scanning electron microscopy and energy-dispersive X-ray spectroscopy (SEM-EDS) measurements (GeminiSEM 300, ZEISS, Germany) were performed to analyzed the elemental composition of zeolite before and after ammonium adsorption.

Zeolite column breakthrough tests were conducted for nonreactive tracer experiments (Cl⁻ as tracer) and for ammonium permeation experiments (detailed in the subsequent paragraph), in separate columns. The bulk density and porosity of the zeolite column were 1.3 g/cm³ and 0.6, respectively. A total of 122.9 g zeolite was poured into an acrylic column (10 cm ×4 cm, height × inner diameter) pre-filled with water to ensure saturation. For the nonreactive tracer (Cl⁻) experiment, 100 mg/L NaCl solution was pumped into zeolite column from the bottom at flow rates of 1 and 2 mL/min, respectively. The effluent solution was collected by the automatic fraction collector every 10 min, and was later tested for Cl⁻ concentration via ion chromatography. The two unknowns, namely the longitudinal mechanical dispersivity (α_L) and effective diffusion coefficient (D^*) of the zeolite matrix can be calculated by two sets of D_{hd} and v (Eq. (3)), which were obtained by fitting Cl⁻ breakthrough curves at flow rates of 1 and 2 mL/min, respectively. The calculated D^* and α_L were assumed also applicable for the hydrodynamic behaviors of NH_4^+ (Brusseau, 1993; de Smedt and Wierenga, 1984; Klotz et al., 1980; Biggar and Nielsen, 1962; Robbins, 1989).

The density, porosity, zeolite weight and size of columns used for ammonium permeation experiments were the same as those in nonreactive tracer experiments. For the ammonium permeation experiments, ammonium solutions (NH_4Cl) of 200, 1000, 2000 mg/L were peristaltically pumped from the bottom at flow rate of 2 mL/min. The effluent solution was collected from column top by an automatic fraction collector at time intervals of 10 min.

The 1-D transport of non-reactive tracer in saturated porous media can be described by advection–dispersion equation as Shackelford and Rowe (1998), Brusseau (1993) and Zheng and Bennett (2002):

$$\theta \frac{\partial C}{\partial t} = D_{hd}\theta \frac{\partial^2 C}{\partial z^2} - q \frac{\partial C}{\partial z} \tag{2}$$

where θ is the volumetric water content of porous medium; C is the solute concentration, in mg/L; t is time, in second; D_{hd} is hydrodynamic dispersion coefficient, in m²/s; q is Darcy's velocity, in m/s; z is the axial distance, in meter.

$$D_{hd} = D^* + \alpha_L v \tag{3}$$

where D^* is effective diffusion coefficient, in m²/s; α_L is longitudinal dispersivity of zeolite matrix, in meter; v is seepage velocity, in m/s.

$$v = \frac{q}{\theta} \tag{4}$$

Hydrodynamic dispersion coefficient (D_{hd}) can be obtained by fitting the breakthrough curves of non-reactive tracer (Cl⁻) (Eq. (2)) at a given flow rate (i.e., seepage velocity). For two unknowns (D^* and α_L), two sets of Eq. (3) are required,

which mandates 2 flow rates (Brusseau, 1993; de Smedt and Wierenga, 1984; Klotz et al., 1980; Biggar and Nielsen, 1962; Robbins, 1989):

$$
\begin{cases} D_{hd1} = D^* + \alpha_L \times v_1 \\ D_{hd2} = D^* + \alpha_L \times v_2 \end{cases} \Rightarrow \begin{cases} \alpha_L = \dfrac{D_{hd1} - D_{hd2}}{v_1 - v_2} \\ D^* = \dfrac{D_{hd2} \times v_1 - D_{hd1} \times v_2}{v_1 - v_2} \end{cases}
\tag{5}
$$

The analytical solution to Eq. (2) is (Shackelford and Rowe, 1998):

$$
\frac{C(L, t)}{C_0} = \frac{1}{2} \left[erfc \left(\frac{L - vt}{2\sqrt{D_{hd}t}} \right) + \exp \left(\frac{vL}{D_{hd}} \right) \times erfc \left(\frac{L + vt}{2\sqrt{D_{hd}t}} \right) \right]
\tag{6}
$$

under the following initial and boundary conditions:

$$
\begin{cases} C(z, 0) = 0 \\ C(0, t) = C_0 \\ C(\infty, t) = 0 \end{cases}
\tag{7}
$$

Eq. (2) can also be solved numerically e.g., by PHREEQC (USGS, USA).

Instantaneous equilibrium was often assumed to be reached in mass transport simulation, which also considered advection, diffusion and mechanical dispersion:

$$
R_d \frac{\partial C}{\partial t} = D_{hd} \frac{\partial^2 C}{\partial z^2} - v \frac{\partial C}{\partial z}
\tag{8}
$$

where R_d is the retardation factor derived from the adsorption isotherm between ammonium and zeolite:

$$
R_d = 1 + \frac{\partial (\rho_b S)}{\partial (\theta C)}
\tag{9}
$$

ρ_b is the dry density, in g/cm^3; and S is the solute content adsorbed onto the solid phase.

The mass transfer equation considering kinetic adsorption can be expressed as Shackelford and Rowe (1998) and Zheng and Bennett (2002):

$$
\theta \frac{\partial C}{\partial t} = D_{hd} \theta \frac{\partial^2 C}{\partial z^2} - q \frac{\partial C}{\partial z} - \frac{\partial (\rho_b S)}{\partial t}
\tag{10}
$$

The 3rd term on the right-hand side represents kinetic adsorption process.

The solution of solute (NH_4^+) transportation in a porous medium requires 3 sets of parameters, the equilibrium adsorption isotherms, the kinetic rate constants, and the hydrodynamic constants (i.e., D^*, α_L). The first two sets of parameters were obtained via batch tests, and the 3rd set of parameters was obtained by tracer tests. The partial differential equation (Eq. (10)) usually was solved numerically, in this study using PHREEQC program (USGS, USA).

The output NH_4^+ concentration at any given time and distance from the starting point provides guidance for barrier performance prediction, monitoring, as well as replacement and regeneration.

3. Results and discussion

Mineralogical and elemental composition of zeolite

The results of XRD pattern and mineralogical compositions of original zeolite were shown in Fig.S1 and Table S1. The mineralogical composition of zeolite was 40.6% mordenite, 19.7% clinoptilolite, 16.3% quartz, 12.7% kaolinite, 8.8% cristobalite and 1.9% zeolite group. Because the original zeolite sample was mainly composed of zeolite minerals, namely clinoptilolite and mordenite, and the cation exchange mechanism for ammonium adsorption by zeolite minerals has been proven by extensive researches, the cation exchange was the mechanism for attenuation of ammonium in this study (Chen et al., 2022; Saltali et al., 2007; Cruz et al., 2019; Karadag et al., 2007, 2008; Obiri-Nyarko et al., 2014).

The surface morphology and elemental composition of the zeolite before and after ammonium adsorption were shown in Fig.S2. It can be obtained from Fig.S2(E) that after the ammonium adsorption, the content of cations in zeolite decreased from 0.34, 1.49, 0.12% to 0.2, 1.31, 0.05% for Na, K and Ca, respectively, and the content of nitrogen in zeolite increased from 0.95% to 2.38%, suggesting the cation exchange was the main mechanism for ammonium attenuation (Chen et al., 2022; Saltali et al., 2007; Cruz et al., 2019; Karadag et al., 2007, 2008; Obiri-Nyarko et al., 2014; Bate et al., 2022; Zhan et al., 2022).

Adsorption Kinetics

Adsorption equilibrium isotherm was found to be best described by Langmuir isotherm (details in S.I.). The fitted parameters of both Langmuir and Freundlich isotherms were presented in Table 1.

The adsorption kinetic reaction of ammonium on zeolite can be described as Du et al. (2005), Ho (2006) and Lin et al. (2013):

$$
Site^- + NH_4^+ \rightarrow SiteNH_4
\tag{11}
$$

Table 1
The fitted parameters of Langmuir and Freundlich isotherms (K_L, S_m: Langmuir constants; a_f, b_f: Freundlich constants; R^2: determination coefficient.)

Langmuir isotherm			Freundlich isotherm		
S_m (mg/g)	K_L (L/mg)	R^2	a_f (mg/g)	b_f	R^2
14.2	0.05	0.9491	5.112	0.123	0.3961
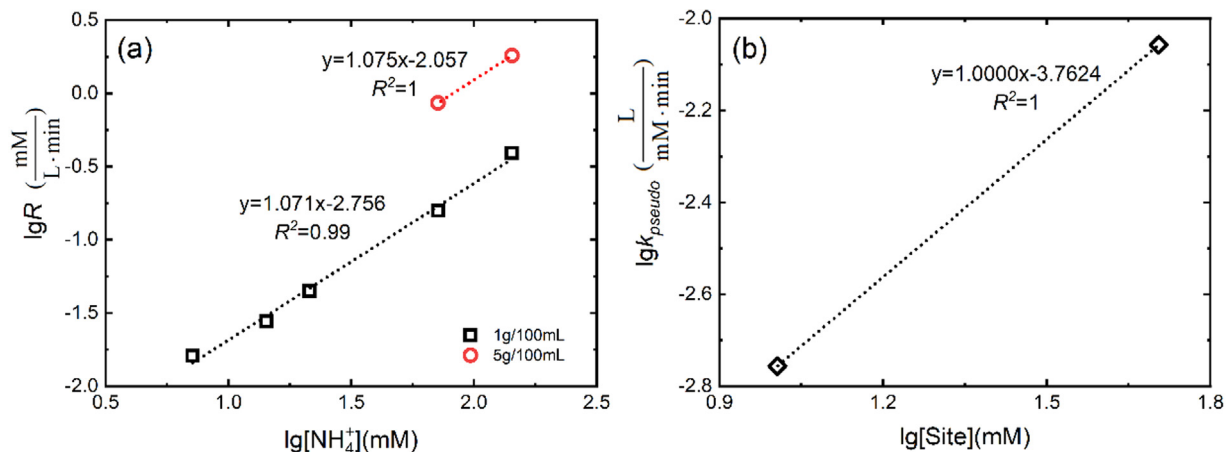
Fig. 1. Experimental data for the determination of the reaction exponents (*a* and *b*) with respect to (a) NH_4^+ and (b) zeolite adsorption site at zeolite dosages of 1 g/100 ml and 5 g/100 ml.

The rate of reaction (R) depends on both the ammonium concentration and the number of adsorption sites of zeolite, which is generally expressed as Eitel et al. (2018), Cavazos et al. (2018) and Taillefert and Gaillard (2002):

$$R = \frac{d[SiteNH_4]}{dt} = -\frac{d[Site]}{dt} = -\frac{d[NH_4^+]}{dt} = k[Site]^a[NH_4^+]^b \qquad (12)$$

where k is the overall rate constant, a and b represent the exponents of the zeolite adsorption site ([Site], mM) and the ammonium concentration ([NH_4^+], mM). Given constant dosage of zeolite, the rate of ammonium adsorption could be simplified into a pseudo-order kinetic model (Eitel et al., 2018; Cavazos et al., 2018; Taillefert and Gaillard, 2002):

$$R = k_{pseudo}[NH_4^+]^b \qquad (13)$$

where

$$k_{pseudo} = k[Site^-]^a \qquad (14)$$

is the apparent rate constant. From Eq. (13), the exponent b can be determined as the slope of the $\lg(R)$-$\lg[NH_4^+]_0$ (log of the initial ammonium concentration) straight line (Eitel et al., 2018; Cavazos et al., 2018; Taillefert and Gaillard, 2002). The initial rate was calculated using the [NH_4^+] evolution over time curve during the initial 10%–15% of the adsorbed NH_4^+ (Eitel et al., 2018; Cavazos et al., 2018; Taillefert and Gaillard, 2002). The calculated exponent b ranges from 1.071 to 1.075 (Fig. 1a), suggesting the first-order kinetic reaction with respect to NH_4^+.

Exponent a can be calculated by fitting Eq. (15):

$$\lg k_{pseudo} = \lg k + a \lg[Site^-] \qquad (15)$$

where a is the slope of the $\lg k_{pseudo} - \lg[Site^-]$ straight line (Fig. 1b), yielding $a = 1.000$, suggesting the first-order reaction rate with respect to the molarity of available zeolite adsorption site.

The overall reaction rate (R) is determined from Eq. (12), suggesting an overall second-order kinetic reaction for the adsorption of ammonium on zeolite:

$$R = -\frac{d[NH_4^+]}{dt} = k[Site^-][NH_4^+] \qquad (16)$$

where $k = 0.1728$ L/(min mol). Then the concentration of NH_4^+ versus time relationship can be obtained by integrating Eq. (16). Given the assumption that monolayer adsorption sites were dispersed uniformly on the zeolite surfaces (S.I., the assumption of Langmuir isotherm) and the amount of adsorption site was determined by cation exchange capacity (CEC,
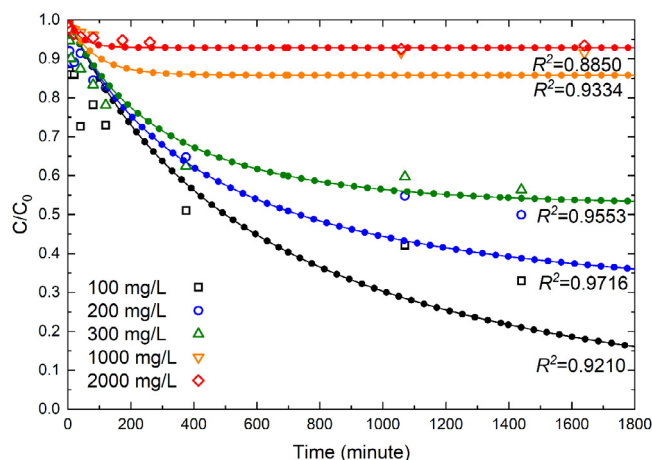
Fig. 2. Experimental (open markers), numerical (solid lines) and analytical (solid markers) results of the temporal evolution of normalized NH_4^+ concentration in aqueous solution with initial NH_4^+ of 100, 200, 300, 1000 and 2000 mg/L. Note: the numerical results nearly coincided with the analytical results.

in mg NH_4^+/g zeolite), Eq. (17) could be derived:

$$-\frac{dC}{dt} = k \times \left(CEC \times \frac{m}{V} - C_0 + C \right) \times C \tag{17}$$

where C represented $[NH_4^+]$. The Eq. (17) could be integrated with the initial condition, as shown in Eq. (18):

$$\begin{cases} \int \frac{dC}{\left(CEC \times \frac{m}{V} - C_0 + C \right) \times C} = -\int k dt \\ C(t=0) = C_0 \end{cases} \tag{18}$$

The explicit analytical solution of Eq. (16) is:

$$C = \frac{\left(CEC \times \frac{m}{V} - C_0 \right) \times C_0}{CEC \times \frac{m}{V} \times \exp\left[\left(CEC \times \frac{m}{V} - C_0 \right) \times kt \right] - C_0} \tag{19}$$

If abundant zeolite was available (i.e. abundant adsorption site), e.g., in a column breakthrough test at initial moment, the Eq. (19) could be simplified:

$$C = C_0 \times \exp\left[-\left(CEC \times \frac{m}{V} - C_0 \right) \times kt \right] \tag{20}$$

which is the typical first-order reaction rate solution (Suprihatin et al., 2020).

On the other hand, if abundant NH_4^+ is available, such as in a batch test with high initial NH_4^+ concentration, the Eq. (19) could be simplified:

$$S = CEC \times \left[1 - \exp\left(-C_0 \times kt \right) \right] \tag{21}$$

which is the typical pseudo-first-order reaction rate solution (Soetardji et al., 2015; Ivanova et al., 2010).

Batch Test Verification

Batch tests were performed simulating NH_4^+ adsorption onto zeolite at initial concentration of 100, 200, 300, 1000, 2000 mg/L, respectively. The normalized $[NH_4^+]$-time evolution relationship was plotted in Fig. 2. $[NH_4^+]$-time evolution curves obtained from the analytical solution of the proposed kinetic method (Eq. (19)) and from PHREEQC simulation were plotted for comparison. The kinetics method yields good C/C_0-time curves, with R^2 range of 0.89–0.97. C/C_0-time curves predicted by PHREEQC, essentially by the same kinetic parameters, also yields the same curves as the analytical solution which validated the ability to simulate kinetic adsorption in PHREEQC program.

Hydrodynamic Features

The hydrodynamic parameters in a zeolite column, namely the effective diffusion coefficient (D^*) and the longitudinal mechanical dispersivity (α_L), were determined by trial-and-error method with high R^2 values (0.9392 and 0.9494), which used PHREEQC to satisfy Eqs. (1)–(2) in two breakthrough instances (1 and 2 mL/min), and then the results were verified by the analytical solution of Eq. (2) (i.e. Eq. (6)) as shown in Fig. 3. The calculated D^* was 1×10^{-9} m^2/s, which was within the range of 1.015×10^{-9} m^2/s to 1.421×10^{-9} m^2/s for D^* of Cl^- migration in a coarse-grained matrix (Shackelford and Rowe, 1998). The calculated longitudinal dispersivity α_L was 8×10^{-3} m, which was similar to the α_L(8.8×10^{-3} m) of a
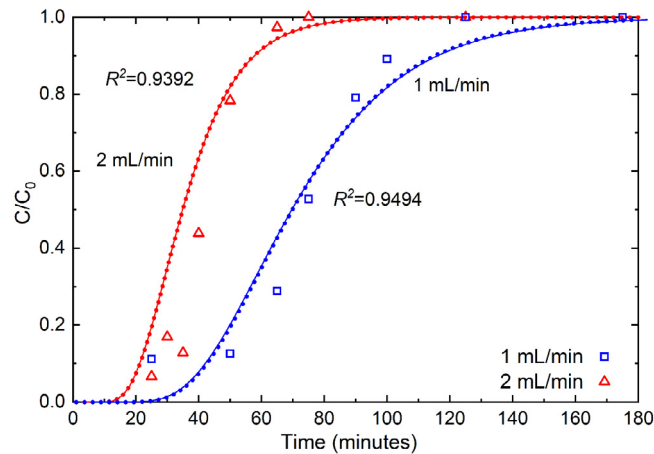
Fig. 3. Column breakthrough curves of Cl⁻ tracer tests. Markers: experimental data, solid lines: the simulation results of PHREEQC, dot lines: analytical solution.
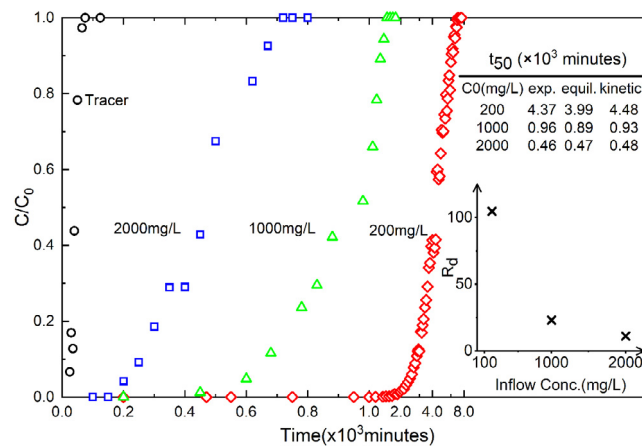

Fig. 4. Experimental ammonium (NH_4^+) breakthrough curves with influent concentrations of 200, 1000, 2000 mg/l. The flow rate of both non-reactive tracer (Cl⁻) and reactive (NH_4^+) permeation experiments was 2 mL/min.

tracer migration in rock column with grain size of 1–2 mm, the same as that of the zeolite used in this study (Klotz et al., 1980). It is worth noting that at a flow rate of 2 mL/min, a mere of 0.28% of the solute disperses via effective diffusion (D^*), while the majority of Cl⁻ disperses via longitudinal mechanical dispersion (99.72%). The latter process (mechanical dispersion), which is solute independent, could then be applied to NH_4^+ breakthrough zeolite process simulation under similar flowrates (Brusseau, 1993; Delgado, 2006).

NH_4^+ Breakthrough Behaviors

The ammonium breakthrough curves were retarded as compared to that of the chloride tracer (Fig. 4) due to adsorption process (Mojid and Vereecken, 2005). Assuming instantaneous equilibrium, the retardation factors (R_d) were defined as the ratio of the velocity of nonreactive tracer to the average velocity of reactive solute (Eq. (22)):

$$R_d = \frac{L/t_{50}^{Cl^-}}{L/t_{50}^{NH_4^+}} = \frac{t_{50}^{NH_4^+}}{t_{50}^{Cl^-}} \tag{22}$$

where L is the length of column; t_{50} is the time when effluent solute concentration reaches $0.5C_0$. The calculated R_d values were 104.6, 23.0, 11.1 for the influent NH_4^+ concentrations of 200, 1000 and 2000 mg/L, respectively (Fig. 4, inset) (Mojid and Vereecken, 2005; USEPA, 1999; Shackelford, 1991; Cao et al., 2019). The R_d decreased with increasing NH_4^+ concentrations suggesting the adsorption sites could be saturated with less pore volumes of solution.

Ammonium transport through zeolite column at the influent concentration of 200, 1000, 2000 mg/L simulated with instantaneous equilibrium assumption yields R^2 range of 0.712–0.863 (Fig. 5), which is not satisfactory. The residence time of NH_4^+ in zeolite column was 38 min (1 pore volume divided by flow rate), while the equilibrium time for full

Table 2

The parameters for simulation of ammonium transport through zeolite using the Langmuir equilibrium model and overall kinetic model in PHREEQC for the influent ammonium concentration of 200, 1000 and 2000 mg/L (v_s: seepage velocity; α_L: zeolite's longitudinal dispersivity; K_L, S_m: Langmuir constants; k: overall rate constant; R^2: determination coefficient for the regression of experimental data versus simulation results.)

C_0	Langmuir equilibrium model						Overall kinetic model				
	v_s	α_L	D^*	S_m	K_L	R^2	v_s	α_L	D^*	k	R^2
mg/L	m min^{-1}	m	$\times 10^{-9}$ m^2/s	mg/g	L/mg		m/ min	m	$\times 10^{-9}$ m^2/s	L/(min · mol)	
200	0.265	0.008	1	14.2	0.05	0.863	0.265	0.008	1	0.1728	0.980
1000	0.265	0.008	1	14.2	0.05	0.843	0.265	0.008	1	0.1728	0.978
2000	0.265	0.008	1	14.2	0.05	0.712	0.265	0.008	1	0.1728	0.940

NH_4^+ adsorption on zeolite in batch tests ranged from 300 to over 1000 min (Fig. 2). This means that the adsorption equilibrium was not reached because of the relatively high seepage velocity compared with the kinetic adsorption rate (Shackelford and Rowe, 1998; Jellali et al., 2010). Therefore, using the instantaneous adsorption model to predict the ammonium breakthrough curves would overestimate the adsorption rate and underestimate the actual extent of the NH_4^+ propagation (Shackelford and Rowe, 1998). Given the low adsorption rate of the kinetic model, as compared to the instantaneous equilibrium model, the unabsorbed ammonium due to relatively fast transportation process led to early ammonium arrival (Fig. 5a), which agrees with prior observations (Jellali et al., 2010; Šimůnek et al., 2006). On the other hand, simulation results with kinetic adsorption model yields R^2 range of 0.940–0.980 for three inlet NH_4^+ concentrations, which are better than those (0.712–0.863) obtained by the instantaneous equilibrium model (Table 1, Fig. 5). This comparison substantiated the kinetic nature of NH_4^+ adsorption onto zeolite sites, which is the rate-limiting step for the NH_4^+ transportation.

The deviation between the simulated breakthrough curves by kinetic-based method and the measured ones appeared at high influent NH_4^+ concentrations (1000 and 2000 mg/L), which were postulated to be due to the following reasons. Firstly, the intraparticle/film diffusion processes of NH_4^+ into zeolite matrix were underestimated by the D^* and α_L coefficients obtained from Cl$^-$ tracer test, given the possible Columbian repulsion between Cl$^-$ anions and negatively-charged zeolite lattices, which limits the Cl$^-$ diffusion through the cavity of zeolite (Karadag et al., 2007; Barczyk et al., 2014; Alver and Metin, 2012). Secondly, the adsorption sites located on zeolite surfaces were sufficient for adsorbing low concentration (200 mg/L) NH_4^+ cations in a column test, similar to the case scenarios in a batch test where the relative abundant NH_4^+ cations (100 to 2000 mg/L) saturated (both on surfaces and inside the intra-aggregate spaces) quickly in a few zeolite grains. In another word, intra-aggregate transportation is not the rate-limiting step for both the batch tests and the column test with low influent NH_4^+ concentration (200 mg/L). For the column breakthrough tests with high influent NH_4^+ concentrations (1000, 2000 mg/L), on the contrary, surface zeolite sites were not sufficient, and NH_4^+ needed to diffuse into the intra pores of zeolite, the rate of which was then limited by the intra-aggregate diffusion process, which was not reflected by either kinetic parameters from a batch test or the Cl$^-$ tracer test. This inherently rendered an overestimation of NH_4^+ adsorption and the early arrival of the breakthrough curves, as revealed by the reduction in determination coefficient (R^2) at high influent NH_4^+ concentrations (Fig. 5b–c) (Shackelford and Rowe, 1998; Zheng and Bennett, 2002; Shackelford, 1991; Jellali et al., 2010).

Advantages of the proposed kinetic-based method

The advantages of the above-proposed kinetic-based method for NH_4^+ adsorption on zeolite are essentially the soundness of the theoretical foundation and the robust applicability to a variety of field conditions. The method was founded on 1D mass transport theory and chemical reaction kinetics, and all the hydrodynamic parameters and kinetic model parameters are constants independent of field conditions, such as NH_4^+ concentration, flow velocity, and content of zeolite. In another word, R_d calibration for flow velocity and NH_4^+ concentration is no longer needed.

Comparison between kinetic-based method and conventional methods

Conventional PRB thickness design methods include maximum adsorption method and residence time method (Obiri-Nyarko et al., 2014; Chen et al., 2012; Gavaskar, 1999). The maximum adsorption method assumes full utilization of the zeolite adsorption capacity for NH_4^+ in accordance with adsorption isotherm. The maximum adsorption method considers only the adsorption capacity of the zeolite at equilibrium, not the hydrodynamic and kinetic adsorption processes. The residence time is the time required for the reaction between contaminated groundwater and reactive material to achieve the treatment goals, and is often calculated by the number of half-lives (time required for concentration reduction of 50%) required to achieve target breakthrough concentration (10% in this study, Woinarski et al., 2006) (Obiri-Nyarko et al., 2014). The residence time method assumes first-order chemical reaction and neglects adsorbate saturation. Above two methods are not always the case in reality. On the contrary, the proposed kinetic-based design method incorporated both the chemical kinetics and hydrodynamic processes, which overcame the shortcomings of the conventional methods. Comparison between conventional methods and the proposed method were compiled in Table 3:
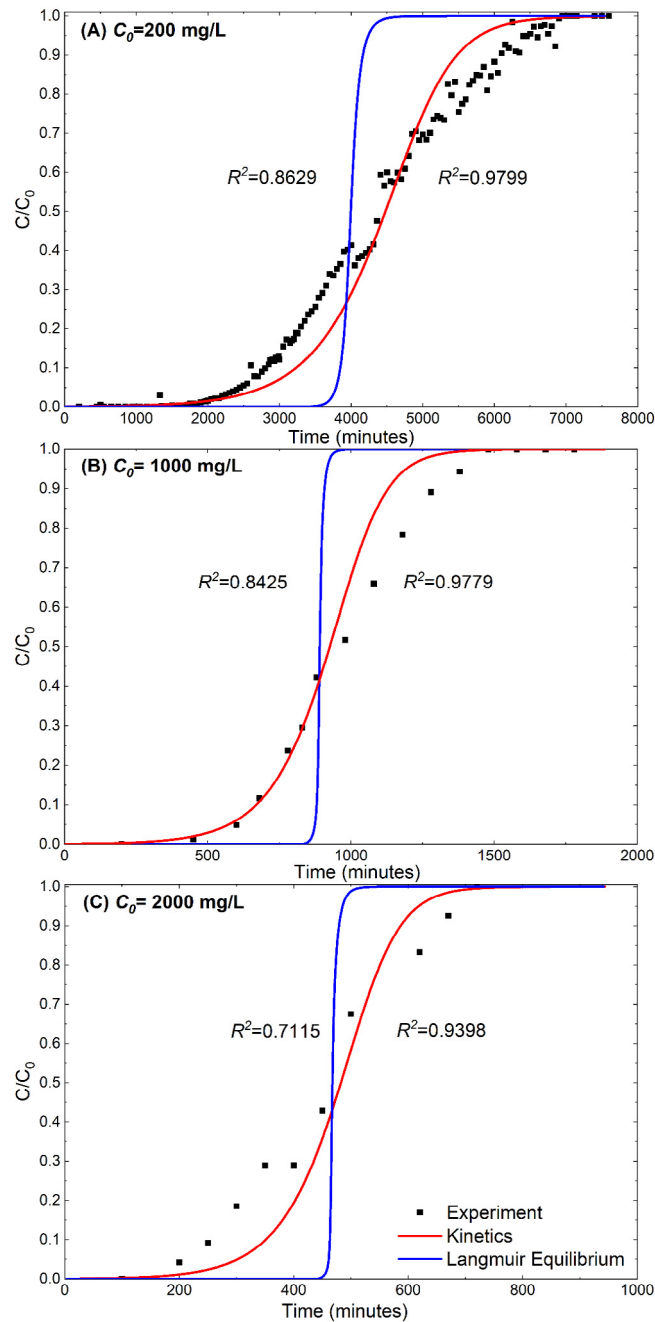
Fig. 5. Experimental breakthrough curves (markers) and simulated breakthrough curves based on Langmuir equilibrium model (blue solid line) and overall kinetic model (red solid line) of the influent ammonium concentration of (A) 200 mg/L, (B) 1000 mg/L, (C) 2000 mg/L. (For interpretation of the references to color in this figure legend, the reader is referred to the web version of this article.)

4. Case study

A multi-layer PRB containing activated carbon (AC) layer and zeolite layer was designed to be installed at the downstream of Tianziling Landfill which was located at a valley in Hangzhou, China to remediate the groundwater containing multi-contaminant. Tianziling Landfill started operation in 1991 for primary municipal solid wastes, and closed in 2007. The groundwater contaminated by the leachate of Tianziling Landfill contained high concentration of ammonium and chemical oxygen demand (COD). The field groundwater was collected to permeate the AC column. Based on the laboratory AC column experiment result as shown in Fig.S4, AC have high affinity for COD while it could hardly retard the

Table 3
Comparison between conventional methods and proposed method.

Methods	Process			
	Advection	Hydrodynamic dispersion	Adsorption	
			Equilibrium	Kinetics
Residence time method	√	×	×	√
Maximum adsorption method	√	×	√	×
Proposed method	√	√	×	√

ammonium. The COD was treated before the ammonium in the AC layer. Up to 85% of the COD in the inflow of PRB was removed by oxidation methods (including O_3 micro-nano bubbles (MNBs) and Fenton technique). While the residual COD was adsorbed by the AC layer. The particle sizes of zeolite and AC used in this case study were similar at 1–2 mm, which corresponding to permeability coefficients of 1.1 cm/s. Given the relatively large particle sizes and the high permeability, removal of COD is unlikely to clog or cause preferential flow of the PRB (not observed, too). Therefore, the hydrodynamic properties of AC layer have little to none influence on the flow to zeolite layer of the PRB. Therefore, the containment of COD in groundwater was assumed to be achieved by the AC layer, and the groundwater ammonium concentration was used to calculated the thickness of zeolite layer. In July 2022, the ammonium concentration of its neighboring downstream zone was approximately 135 mg/L, which exceeded standard limits of groundwater quality (1.5 mg/L, GB/T 14848-2017). The zeolite PRB was planned to be installed perpendicular to the groundwater flow direction, downstream of the landfill and the PRB was planned to build to a depth and width that over-encompasses the vertical and horizontal dimensions of the contaminant plume, and the insertion depth of PRB into the impervious layer (aquitard) should be 30 cm or sufficient to elongate the seepage path underneath PRB to prevent circumventing (Ott, 2000; Gavaskar et al., 1998; Powell et al., 1998). The Darcy velocity of the groundwater was 0.29 m/d, and the designed seepage velocity within PRB was 0.49 m/d.

Based on Langmuir isotherm obtained from batch test, the thickness of PRB (H) by maximum adsorption method can be calculated by:

$$H = \frac{q \cdot C \cdot T}{S_e \cdot \rho_b} \tag{23}$$

where T (day) is the service life of PRB. Given the site condition of Tianziling Landfill and a design service life of 2 years, H was 1.54 m.

The residence time was determined by the number of half-lives required to reduce the influent concentration of the contaminant to below its threshold breakthrough concentration, which was $0.1C_0$ in this study (Obiri-Nyarko et al., 2014; Gavaskar, 1999):

$$t_{res} = N \times t_{0.5} \times u_1 \times u_2 \times SF \tag{24}$$

$$H = q \times t_{res} \tag{25}$$

where N is the number of half-lives required to reduce the influent concentration to below $0.1C_0$, $N = 4$ in this study, $t_{0.5}$ is the half-life of the reaction between ammonium and zeolite obtained from batch test by first-order kinetic model, $t_{0.5} = 0.127d$, u_1 was the temperature correction factor which was assumed to be 2, u_2 was the bulk density correction factor which was assumed to be 1.5, SF was the safety factor which was assumed to be 2 (Chen et al., 2012; Gavaskar, 1999). The thickness of the PRB based on the residence time method was calculated to be 0.88 m for Tianziling Landfill.

With the overall kinetics model (Eq. (10)) and hydrodynamic parameters obtained from tracer test (Table 1), a new method for calculating the thickness of PRB for Tianziling Landfill was proposed as follows. Indeed, there were multiple cations in real contaminated groundwater. And it is true that the other cations, such as Na^+ and K^+, compete with NH_4^+ in the adsorption process onto zeolite. Per this situation, additional zeolite breakthrough experiment was performed with collected real groundwater from Tianziling Landfill site. The chemical speciation of the cations of the real groundwater was tabulated in Table 4, with the main cations of NH_4^+, Ca^{2+}, K^+, Mg^{2+}, and Na^+. Among these cations, bivalent cations (Ca^{2+} and Mg^{2+}) were mostly adsorbed by the preceding AC layer due to the strong adsorption capability of AC. The remaining monovalent cations (K^+, Na^+, NH_4^+) compete for the adsorption site. Lyotropic series (Bohn et al., 2002; Sposito et al., 1984) suggest the selectivity of zeolite site for competing cations as: $K^+ > Na^+ > NH_4^+$, given equal concentration. On the other hand, the actual concentrations of these three monovalent cations are in the order of $K^+ < Na^+ < NH_4^+$. A simple assumption was made that, the molarity of the zeolite adsorbed cations of each type of monovalent cations is proportional to the concentration of this type of monovalent cation. Then, the adsorbed NH_4^+ accounts for 45% of the available zeolite adsorption sites.

This reduction factor (45%) for NH_4^+ adsorption onto zeolite was introduced in the numerical simulation program, and yielded good fit of the breakthrough curve with $R^2 = 0.9573$ (Fig. 6). This good agreement between the experiments and the numerical simulation validated the above assumption in this case study. Numerical solver, PHREEQC was used to incorporate both the chemical kinetics and hydrodynamic processes with the parameters listed in Table 2. The length of cells in PHREEQC were set to 0.01 m, and the time step which was equal to length of cell divided by seepage velocity

Table 4
Concentration of cations of the collected real groundwater in Tianziling Landfill site.

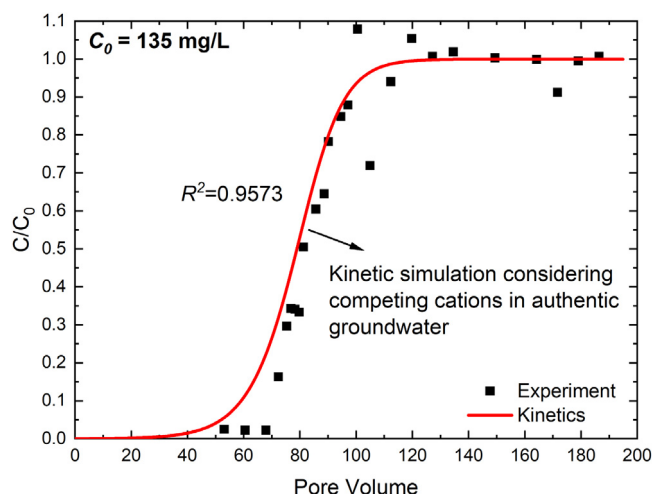| Cations	Concentration (mmol/L)
NH_4^+	9.64
K^+	2.86
Na^+	9.06
Ca^{2+}	1.08
Mg^{2+}	0.40

Fig. 6. Experimental breakthrough curve of NH_4^+ using the real groundwater (scatters) and simulated NH_4^+ breakthrough curve based on kinetic simulation considering competing cations in authentic groundwater.

Table 5
The parameters for PRB design based on ammonium transport simulation considering overall kinetic model.

C_0 mg/L	v_s m/day	α_L [a] m	D^* $\times 10^{-9}$ m²/s	k L/(min · mol)	H m
135	0.49	0.1	1	0.1728	4.45

[a]The longitudinal dispersivity was dependent on scale and the dispersivity used for PRB design were assumed to be linear with that obtained from laboratory tracer test Gelhar et al. (1992).

was 1763 s. To meet the PRB service life requirement (2 years), the number of cells (the PRB thickness was equal to the number of cells times the length of cells) was searched by trial-and-error method.

Given $0.1C_0$ breakthrough criterion (Woinarski et al., 2006), the calculated thickness of the PRB was 4.45 m, which was thicker than those calculated by either maximum adsorption method (1.54 m) or residence time method (0.88 m). The newly proposed method gives a safer design. The distribution of NH_4^+ concentration along PRB thickness at given time could also be obtained (Fig. 7), which provides a basis for performance monitoring and filling material replacement (see Fig. 7 and Table 5).

5. Conclusion

The major findings in this study were summarized as follows:

(1) Based on two-variables batch tests for NH_4^+ adsorption on zeolite, the adsorption kinetic parameters (Eq. (16)) were obtained: the overall kinetic rate constant $k = 0.1728$ L/(min mol), the adsorption reaction rate was found to be first-order with respect to both NH_4^+ concentration (exponent $a = 1.07$) and the molarity of the available adsorption sites of the zeolite (exponent $b = 1.00$).

(2) Hydrodynamic parameters dictating both diffusion (effective diffusion coefficient $D^* = 1 \times 10^{-9}$ m²/s) and longitudinal mechanical dispersion ($\alpha_L = 8 \times 10^{-3}$ m) processes were obtained by Cl^- tracer column breakthrough tests. Mechanical dispersion process, which is solute independent, was the major hydrodynamic transportation mechanism at experimental conditions in this study. This validates the applicability of hydrodynamic parameters obtained from Cl^- anions to the transport of NH_4^+ cations.
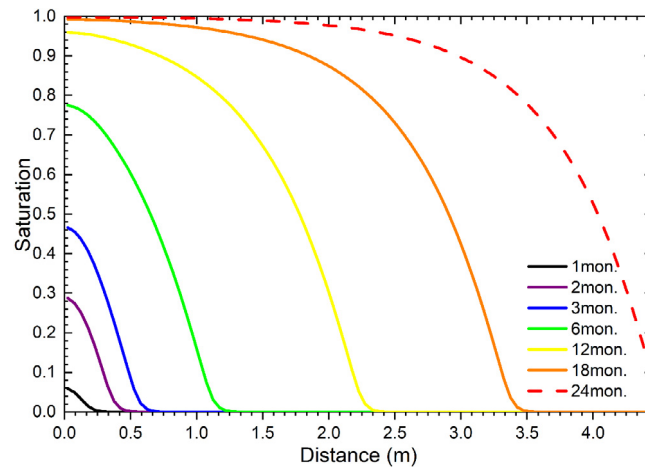
Fig. 7. Monthly ammonium concentration distribution in the PRB with the barrier in service life of 2 years.

(3) Good agreement between the proposed kinetics-based NH_4^+ transport simulation method and column tests substantiated the advantages of the newly-proposed kinetic-based method.

(4) The kinetic-based method was used for designing the thickness of a permeable reactive barrier (PRB) for remediating NH_4^+ leached from Tianziling Landfill. The calculated PRB thickness was 4.45 m, which was more conservative than those calculated from traditional methods.

Summary of symbols and parameters used in this study

Variable	Unit	Description
S_e	mg/g	Equilibrium adsorbed NH_4^+ concentration
S	mg/g	Adsorbed NH_4^+ concentration
C_0	mg/L	Initial NH_4^+ concentration
C_e	mg/L	Equilibrium NH_4^+ concentration
V	L	Solution volume
m	g	Weight of zeolite
θ	–	Volumetric water content
t	second	Time
z	m	Axial distance
q	m/s	Darcy's velocity
v	m/s	seepage velocity
D_{hd}	m^2/s	Hydrodynamic dispersion coefficient
D^*	m^2/s	Effective diffusion coefficient
α_L	m	Longitudinal dispersivity
R_d	–	Retardation factor
ρ_b	g/cm^3	Dry density of zeolite
k	L/(min mol)	Overall rate constant
k_{pseudo}	1/min	Apparent rate constant
a	–	Exponents of the zeolite adsorption site
b	–	Exponents of the ammonium concentration
S_m	mg/g	Maximum adsorption capacity of Langmuir isotherm
K_L	L/mg	Langmuir adsorption constant
a_f	mg/g	Multilayer adsorption capacity of Freundlich isotherms
b_f	–	Adsorption intensity of Freundlich isotherms
CEC	meq/g	Cation exchange capacity of NH_4^+ in absence of competing cations.

CRediT authorship contribution statement

Yi-Xin Yang: Conceptualization, Methodology, Investigation, Software, Writing – original draft. **Jia-Kai Chen:** Investigation. **Li Zhao:** Investigation. **Yu-Qing You:** Investigation. **Ze-Jian Chen:** Investigation. **Jun-Nan Cao:** Investigation. **Fei**

Declaration of competing interest

The authors declare the following financial interests/personal relationships which may be considered as potential competing interests: Bate Bate reports financial support was provided by Ministry of Science and Technology of the People's Republic of China. Bate Bate reports financial support was provided by National Natural Science Foundation of China. Bate Bate reports financial support was provided by Overseas Expertise Introduction Project for Discipline Innovation.

Data availability

Data will be made available on request.

Acknowledgments

Appendix A. Supplementary data

Supplementary material related to this article can be found online at https://doi.org/10.1016/j.eti.2023.103020.

References

Alkan, M., Demirbaş, Ö., Doğan, M., 2007. Adsorption kinetics and thermodynamics of an anionic dye onto sepiolite. Microporous Mesoporous Mater. 101, 388–396. http://dx.doi.org/10.1016/j.micromeso.2006.12.007.

Alver, E., Metin, A.ü., 2012. Anionic dye removal from aqueous solutions using modified zeolite: Adsorption kinetics and isotherm studies. Chem. Eng. J. 200–202, 59–67. http://dx.doi.org/10.1016/j.cej.2012.06.038.

Barczyk, K., Mozgawa, W., Król, M., 2014. Studies of anions sorption on natural zeolites. Spectrochim. Acta A Mol. Biomol. Spectrosc. 133, 876–882. http://dx.doi.org/10.1016/j.saa.2014.06.065.

Bate, B., Ye, J., Cao, J., You, Y., Cao, J., Zhang, S., Zhan, L.T., Zhang, C., Hao, N., 2022. The mechanisms and monitoring of zeolite remediating chemical oxygen demand, NH4+, and Pb2+. J. Appl. Geophys. 199, http://dx.doi.org/10.1016/j.jappgeo.2022.104615.

Bhatnagar, A., Kumar, E., Sillanpää, M., 2010. Nitrate removal from water by nano-alumina: Characterization and sorption studies. Chem. Eng. J. 163, 317–323. http://dx.doi.org/10.1016/j.cej.2010.08.008.

Biggar, J.W., Nielsen, D.R., 1962. Some comments on molecular diffusion and hydrodynamic dispersion in porous media. J. Geophys. Res. (1896-1977) 67, 3636–3637. http://dx.doi.org/10.1029/JZ067i009p03636.

Bohn, H.L., Myer, R.A., O'Connor, G.A., 2002. Soil Chemistry. John Wiley & Sons.

Boopathy, R., Karthikeyan, S., Mandal, A.B., Sekaran, G., 2013. Adsorption of ammonium ion by coconut shell-activated carbon from aqueous solution: Kinetic, isotherm, and thermodynamic studies. Environ. Sci. Pollut. Res. 20, 533–542. http://dx.doi.org/10.1007/s11356-012-0911-3.

Bortone, I., Chianese, S., di Nardo, A., di Natale, M., Erto, A., Musmarra, D., 2013. A comparison between pump & treat technique and permeable reactive barriers for the remediation of groundwater contaminated by chlorinated organic compounds. Chem. Eng. Trans. 32, 31–36. http://dx.doi.org/10.3303/CET1332006.

Bortone, I., Erto, A., di Nardo, A., di Natale, M., Santonastaso, G., Musmarra, D., 2014. Design of permeable adsorbing barriers for groundwater protection: Optimization of the intervention. Chem. Eng. Trans. 36, 547–552. http://dx.doi.org/10.3303/CET1436092.

Brusseau, M.L., 1993. The influence of solute size, pore water velocity, and intraparticle porosity on solute dispersion and transport in soil. Water Resour. Res. 29, 1071–1080. http://dx.doi.org/10.1029/92WR02595.

Cai, Q., Turner, B.D., Sheng, D., Sloan, S., 2018. Application of kinetic models to the design of a calcite permeable reactive barrier (PRB) for fluoride remediation. Water Res. 130, 300–311. http://dx.doi.org/10.1016/j.watres.2017.11.046.

Cao, J., Bate, B., Bouazza, A., Deng, W., 2019. Measuring retardation factors of cesium133 and strontium88 cations using column test. J. Geotech. Geoenviron. Eng. 145, 06019009. http://dx.doi.org/10.1061/(ASCE)GT.1943-5606.0002107.

Cavazos, A.R., Taillefert, M., Tang, Y., Glass, J.B., 2018. Kinetics of nitrous oxide production from hydroxylamine oxidation by birnessite in seawater. Mar. Chem. 202, 49–57. http://dx.doi.org/10.1016/j.marchem.2018.03.002.

Chen, L., Wang, C., Zhang, C., Zhang, X., Liu, F., 2022. Eight-year performance evaluation of a field-scale zeolite permeable reactive barrier for the remediation of ammonium-contaminated groundwater. Appl. Geochem. 143, http://dx.doi.org/10.1016/j.apgeochem.2022.105372.

Chen, Z., Zhang, C., Li, H., Zhang, Y., Qiu, J., Lin, T., 2012. On the structure and design of permeable reactive barrier. J. Saf. Environ. 12, 56–61.

Cruz, H., Law, Y.Y., Guest, J.S., Rabaey, K., Batstone, D., Laycock, B., Verstraete, W., Pikaar, I., 2019. Mainstream ammonium recovery to advance sustainable urban wastewater management. Environ. Sci. Technol. 53, 11066–11079. http://dx.doi.org/10.1021/acs.est.9b00603.

de Smedt, F., Wierenga, P.J., 1984. Solute transfer through columns of glass beads. Water Resour. Res. 20, 225–232. http://dx.doi.org/10.1029/WR020i002p00225.

Delgado, J.M.P.Q., 2006. A critical review of dispersion in packed beds. Heat Mass Transf. 42, 279–310. http://dx.doi.org/10.1007/s00231-005-0019-0.

Du, Q., Liu, S., Cao, Z., Wang, Y., 2005. Ammonia removal from aqueous solution using natural Chinese clinoptilolite. Sep. Purif. Technol. 44, 229–234. http://dx.doi.org/10.1016/j.seppur.2004.04.011.

Eitel, E.M., Zhao, S., Tang, Y., Taillefert, M., 2018. Effect of manganese oxide aging and structure transformation on the kinetics of thiol oxidation. Environ. Sci. Technol. 52, 13202–13211. http://dx.doi.org/10.1021/acs.est.8b03993.

Englert, A.H., Rubio, J., 2005. Characterization and environmental application of a Chilean natural zeolite. Int. J. Miner. Process. 75, 21–29. http://dx.doi.org/10.1016/j.minpro.2004.01.003.

Erto, A., Andreozzi, R., di Natale, F., Lancia, A., Musmarra, D., 2009. Experimental and isotherm-models analysis on TCE and PCE adsorption onto activated carbon. Chem. Eng. Trans. 17, 293–298. http://dx.doi.org/10.3303/CET0917050.

Gavaskar, A.R., 1999. Design and construction techniques for permeable reactive barriers. J. Hazard. Mater. 68, 41–71. http://dx.doi.org/10.1016/S0304-3894(99)00031-X.

Gavaskar, A.R., Gupta, N., Sass, B., Janosy, R., OSullivan, D., 1998. Permeable barriers for groundwater remediation.

Gelhar, L.W., Welty, C., Rehfeldt, K.R., 1992. A critical review of data on field-scale dispersion in aquifers. Water Resour. Res. 28, 1955–1974. http://dx.doi.org/10.1029/92WR00607.

Han, Z., Ma, H., Shi, G., He, L., Wei, L., Shi, Q., 2016. A review of groundwater contamination near municipal solid waste landfill sites in China. Sci. Total Environ. 569–570, 1255–1264. http://dx.doi.org/10.1016/j.scitotenv.2016.06.201.

Hao, N., Cao, J., Ye, J., Zhang, C., Li, C., Bate, B., 2021. Content and morphology of lead remediated by activated carbon and biochar: A spectral induced polarization study. J. Hazard. Mater. 411, 124605. http://dx.doi.org/10.1016/j.jhazmat.2020.124605.

Hao, N., You, Y., Zhan, L.T., Bate, B., 2022. Evaluation of aqueous Cd2+ and Pb2+ removal by natural loess using spectral induced polarization and microscopic characterization. Environ. Sci. Pollut. Res. 29, 50500–50514. http://dx.doi.org/10.1007/s11356-022-19307-7.

He, W., Gong, H., Fang, K., Peng, F., Wang, K., 2019. Revealing the effect of preparation parameters on zeolite adsorption performance for low and medium concentrations of ammonium. J. Environ. Sci. (China) 85, 177–188. http://dx.doi.org/10.1016/j.jes.2019.05.021.

Henderson, A.D., Demond, A.H., 2007. Long-term performance of zero-valent iron permeable reactive barriers: A critical review. Environ. Eng. Sci. 24, 401–423. http://dx.doi.org/10.1089/ees.2006.0071.

Ho, Y.S., 2006. Review of second-order models for adsorption systems. J. Hazard. Mater. 136, 681–689. http://dx.doi.org/10.1016/j.jhazmat.2005.12.043.

Ivanova, E., Karsheva, M., Koumanova, B., 2010. Adsorption of ammonium ions onto natural zeolite. J. Univ. Chem. Technol. Metall. 45, 295–302, https://www.researchgate.net/publication/268040187.

Jellali, S., Diamantopoulos, E., Kallali, H., Bennaceur, S., Anane, M., Jedidi, N., 2010. Dynamic sorption of ammonium by sandy soil in fixed bed columns : Evaluation of equilibrium and non-equilibrium transport processes. J. Environ. Manag. 91, 897–905. http://dx.doi.org/10.1016/j.jenvman.2009.11.006.

Karadag, D., Akkaya, E., Demir, A., Saral, A., Turan, M., Ozturk, M., 2008. Ammonium removal from municipal landfill leachate by clinoptilolite bed columns: Breakthrough modeling and error analysis. Ind. Eng. Chem. Res. 47, 9552–9557. http://dx.doi.org/10.1021/ie800434e.

Karadag, D., Koc, Y., Turan, M., Ozturk, M., 2007. A comparative study of linear and non-linear regression analysis for ammonium exchange by clinoptilolite zeolite. J. Hazard. Mater. 144, 432–437. http://dx.doi.org/10.1016/j.jhazmat.2006.10.055.

Katarzyna, P., Mieczyslaw, P., Grzegorz, W., Marzena, L.-S., 2019. Two-objective optimization for optimal design of the multilayered permeable reactive barriers. IOP Conf. Ser: Mater. Sci. Eng. 471, 112044. http://dx.doi.org/10.1088/1757-899X/471/11/112044.

Kjeldsen, P., Barlaz, M.A., Rooker, A.P., Baun, A., Ledin, A., Christensen, T.H., 2002. Present and long-term composition of MSW landfill leachate: A review. Crit. Rev. Environ. Sci. Technol. 32, 297–336. http://dx.doi.org/10.1080/10643380290813462.

Klotz, D., Seiler, K.-P., Moser, H., Neumaier, F., 1980. Dispersivity and velocity relationship from laboratory and field experiments. J. Hydrol. (Amst.) 45, 169–184. http://dx.doi.org/10.1016/0022-1694(80)90018-9.

Liang-tong, Z., Li, Z., Yuqing, Y., Na, H., Bate, B., 2022. Investigation of aqueous Fe (III) and Mn (II) removal using dolomite as a permeable reactive barrier material. Environ. Technol. http://dx.doi.org/10.1080/09593330.2021.2020340.

Lin, L., Lei, Z., Wang, L., Liu, X., Zhang, Y., Wan, C., Lee, D.J., Tay, J.H., 2013. Adsorption mechanisms of high-levels of ammonium onto natural and NaCl-modified zeolites. Sep. Purif. Technol. 103, 15–20. http://dx.doi.org/10.1016/j.seppur.2012.10.005.

Maamoun, I., Eljamal, O., Falyouna, O., Eljamal, R., Sugihara, Y., 2020. Multi-objective optimization of permeable reactive barrier design for Cr(VI) removal from groundwater. Ecotoxicol. Environ. Saf. 200, 110773. http://dx.doi.org/10.1016/j.ecoenv.2020.110773.

Mojid, M.A., Vereecken, H., 2005. On the physical meaning of retardation factor and velocity of a nonlinearly sorbing solute. J. Hydrol. (Amst.) 302, 127–136. http://dx.doi.org/10.1016/j.jhydrol.2004.06.041.

Obiri-Nyarko, F., Grajales-Mesa, S.J., Malina, G., 2014. An overview of permeable reactive barriers for in situ sustainable groundwater remediation. Chemosphere 111, 243–259. http://dx.doi.org/10.1016/j.chemosphere.2014.03.112.

Ott, N., 2000. Permeable reactive barriers for inorganics. http://www.clu-in.org.

Pan, M., Zhang, M., Zou, X., Zhao, X., Deng, T., Chen, T., Huang, X., 2019. The investigation into the adsorption removal of ammonium by natural and modified zeolites: Kinetics, isotherms, and thermodynamics. Water SA 45, 648–656. http://dx.doi.org/10.17159/wsa/2019.v45.i4.7546.

Powell, R.M., Blowes, D.W., Gillham, R.W., Schultz, D., Sivavec, T., Puls, R.W., Vogan, J.L., Powell, P.D., Landis, R., 1998. Permeable Reactive Barrier Technologies for Contaminant Remediation, Vol. 600. US EPA.

Renou, S., Givaudan, J.G., Poulain, S., Dirassouyan, F., Moulin, P., 2008. Landfill leachate treatment: Review and opportunity. J. Hazard. Mater. 150, 468–493. http://dx.doi.org/10.1016/j.jhazmat.2007.09.077.

Robbins, G.A., 1989. Methods for determining transverse dispersion coefficients of porous media in laboratory column experiments. Water Resour. Res. 25, 1249–1258. http://dx.doi.org/10.1029/WR025i006p01249.

Saltali, K., Sari, A., Aydin, M., 2007. Removal of ammonium ion from aqueous solution by natural Turkish (Yildizeli) zeolite for environmental quality. J. Hazard. Mater. 141, 258–263. http://dx.doi.org/10.1016/j.jhazmat.2006.06.124.

Santonastaso, G.F., Erto, A., Bortone, I., Chianese, S., di Nardo, A., Musmarra, D., 2018. Experimental and simulation study of the restoration of a thallium (I)-contaminated aquifer by Permeable Adsorptive Barriers (PABs). Sci. Total Environ. 630, 62–71. http://dx.doi.org/10.1016/j.scitotenv.2018.02.169.

Shackelford, C.D., 1991. Laboratory diffusion testing for waste disposal - A review. J. Contam. Hydrol. 7, 177–217. http://dx.doi.org/10.1016/0169-7722(91)90028-Y.

Shackelford, C.D., Rowe, R.K., 1998. Contaminant transport modeling. Environ. Geotech. 83, 24–25. http://dx.doi.org/10.4324/9780203938485-13.

Shen, H., Wilson, J.T., 2007. Trichloroethylene removal from groundwater in flow-through columns simulating a permeable reactive barrier constructed with plant mulch. Environ. Sci. Technol. 41, 4077–4083. http://dx.doi.org/10.1021/es0626180.

Šimůnek, J., Jacques, D., van Genuchten, M.Th., Mallants, D., 2006. Multicomponent geochemical transport modeling using hydrus-1D and HP1. JAWRA J. Am. Water Resour. Assoc. 42, 1537–1547. http://dx.doi.org/10.1111/j.1752-1688.2006.tb06019.x.

Soetardji, J.P., Claudia, J.C., Ju, Y.H., Hriljac, J.A., Chen, T.Y., Soetaredjo, F.E., Santoso, S.P., Kurniawan, A., Ismadji, S., 2015. Ammonia removal from water using sodium hydroxide modified zeolite mordenite. RSC Adv. 5, 83689–83699. http://dx.doi.org/10.1039/c5ra15419g.

Son, E.B., Poo, K.M., Chang, J.S., Chae, K.J., 2018. Heavy metal removal from aqueous solutions using engineered magnetic biochars derived from waste marine macro-algal biomass. Sci. Total Environ. 615, 161–168. http://dx.doi.org/10.1016/j.scitotenv.2017.09.171.

Sposito, G., et al., 1984. The Surface Chemistry of Soils. Oxford University Press.

Suprihatin, S., Yani, M., Fitriyani, A.L., 2020. Simultaneous recovery of ammonium and phosphate from leachate by using activated zeolite. IOP Conf. Ser. Earth Environ. Sci. 477, http://dx.doi.org/10.1088/1755-1315/477/1/012004.

Taillefert, M., Gaillard, J.-F., 2002. Reactive transport modeling of trace elements in the water column of a stratified lake: iron cycling and metal scavenging. J. Hydrol. (Amst.) 256, 16–34. http://dx.doi.org/10.1016/S0022-1694(01)00524-8.

USEPA, 1999. Understanding Variation in Partition Coefficient, Kd, Values. Volume 1: The Kd Model, Methods of Measurement, and Application of Chemical Reaction Codes. https://www.researchgate.net/publication/233120800.

Wang, Y.F., Lin, F., Pang, W.Q., 2007. Ammonium exchange in aqueous solution using Chinese natural clinoptilolite and modified zeolite. J. Hazard. Mater. 142, 160–164. http://dx.doi.org/10.1016/j.jhazmat.2006.07.074.

Wang, Y., Pleasant, S., Jain, P., Powell, J., Townsend, T., 2016. Calcium carbonate-based permeable reactive barriers for iron and manganese groundwater remediation at landfills. Waste Manage. 53, 128–135. http://dx.doi.org/10.1016/j.wasman.2016.02.018.

Wang, L., Wang, Y., Ma, F., Tankpa, V., Bai, S., Guo, X., Wang, X., 2019. Mechanisms and reutilization of modified biochar used for removal of heavy metals from wastewater: A review. Sci. Total Environ. 668, 1298–1309. http://dx.doi.org/10.1016/j.scitotenv.2019.03.011.

Woinarski, A.Z., Stevens, G.W., Snape, I., 2006. A natural zeolite permeable reactive barrier to treat heavy-metal contaminated waters in Antarctica: Kinetic and fixed-bed studies. Process Saf. Environ. Prot. 84, 109–116. http://dx.doi.org/10.1205/psep.04296.

Ye, J., Chen, X., Chen, C., Bate, B., 2019. Emerging sustainable technologies for remediation of soils and groundwater in a municipal solid waste landfill site – A review. Chemosphere 227, 681–702. http://dx.doi.org/10.1016/j.chemosphere.2019.04.053.

Zhan, L., You, Y., Zhao, L., Hao, N., Bate, B., 2022. A study on the competitive adsorption process of NH4+ and Zn2+ on activated carbon and zeolite. Int. J. Environ. Sci. Technol. http://dx.doi.org/10.1007/s13762-022-04375-6.

Zhang, Y., Cao, B., Yin, H., Meng, L., Jin, W., Wang, F., Xu, J., Al-Tabbaa, A., 2022. Application of zeolites in permeable reactive barriers (PRBs) for in-situ groundwater remediation: A critical review. Chemosphere 308, 136290. http://dx.doi.org/10.1016/j.chemosphere.2022.136290.

Zhao, Y., Niu, Y., Hu, X., Xi, B., Peng, X., Liu, W., Guan, W., Wang, L., 2016. Removal of ammonium ions from aqueous solutions using zeolite synthesized from red mud. Desalination Water Treat. 57, 4720–4731. http://dx.doi.org/10.1080/19443994.2014.1000382.

Zheng, C., Bennett, G.D., 2002. Applied Contaminant Transport Modeling, second ed. Wiley-Interscience, New York.